# Chromatic dispersion compensation and coherent Direct-Sequence OCDMA operation on a single super structured FBG

**Rocío Baños, Daniel Pastor,* Waldimar Amaya, and Victor Garcia-Munoz**

*Institute of Telecommunications and Multimedia Applications (iTEAM), Universidad Politécnica de Valencia, Camino de Vera S/N, 46021 Valencia- Spain*

*dpastor@dcom.upv.es*

**Abstract:** We have proposed, fabricated and demonstrated experimentally a set of Coherent Direct Sequence-OCDMA en/decoders based on Super Structured Fiber Bragg Gratings (SSFBGs) which are able to compensate the fiber chromatic dispersion at the same time that they perform the en/decoding task. The proposed devices avoid the use of additional dispersion compensation stages reducing system complexity and losses. This performance was evaluated for 5.4, 11.4 and 16.8 km of SSMF. The twofold performance was verified in Low Reflectivity regime employing only one GVD compensating device at decoder or sharing out the function between encoder and decoder devices. Shared functionality requires shorter SSFBGs designs and also provides added flexibility to the optical network design. Moreover, dispersion compensated en/decoders were also designed into the High Reflectivity regime employing synthesis methods achieving more than 9 dB reduction of insertion loss for each device.



**OCIS codes:** (060.0060) Fiber optics and optical communications; (060.3735) Fiber Bragg gratings; (230.0230) Optical devices.

## References and links

1. K. Kitayama, X. Wang, and N. Wada, "OCDMA over WDM PON—solution path to gigabit-symmetric FTTH," J. Lightwave Technol. **24**(4), 1654–1662 (2006).
2. X. Wang and N. Wada, "Experimental demonstration of OCDMA traffic over optical packet switching network with hybrid PLC and SSFBG En/decoders," J. Lightwave Technol. **24**(8), 3012–3020 (2006).
3. H. Sotobayashi, W. Chujo, and K. Kitayama, "Transparent virtual optical code/wavelength path network," IEEE J. Sel. Top. Quantum Electron. **8**(3), 699–704 (2002).
4. R. Paul Prucnal, *Optical Code Division Multiple Access: Fundamentals and Applications* (CRC Taylor & Francis, 2006)
5. D. Pastor, W. Amaya, and R. Garcia-Olcina, "Effect of group velocity dispersion on all-optical encoded labels in optical packet networks," in *Proceedings of International Conference on Transparent Optical Networks* (Azores, 2009), 1–4
6. B. Dai and X. Wang, "Novel FBG decoder for simultaneous time domain coherent optical code recognition and chromatic dispersion compensation," IEEE Photon. Technol. Lett. **22**, 1671–1673 (2010).
7. D. Pastor, W. Amaya, R. Baños, and V. Garcia-Munoz, "Simultaneous chromatic dispersion compensation and coherent direct-sequence OCDMA encoding on a single SSFBG device," in *Proceedings of International Conference on Transparent Optical Networks* (Stockholm, 2011), 1–4
8. D. Pastor, W. Amaya, R. García-Olcina, and S. Sales, "Coherent direct sequence optical code multiple Access encoding-decoding efficiency versus wavelength detuning," Opt. Lett. **32**(13), 1896–1898 (2007).
9. X. Wang, K. Matsushima, A. Nishiki, N. Wada, and K. Kitayama, "High reflectivity superstructured FBG for coherent optical code generation and recognition," Opt. Express **12**(22), 5457–5468 (2004).
10. D. Pastor, W. Amaya, and R. Garcia-Olcina, "Design of high reflectivity superstructured FBG for coherent OCDMA employing synthesis approach," Electron. Lett. **43**(15), 824–825 (2007).
11. J. Skaar, Ligang Wang, and T. Erdogan, "On the synthesis of fiber Bragg gratings by layer peeling," IEEE J. Quantum Electron. **37**(2), 165–173 (2001).
12. W. Amaya, D. Pastor, R. Baños, and V. Garcia-Munoz, "WDM-Coherent OCDMA over one single device based on short chip Super Structured Fiber Bragg Gratings," Opt. Express **19**(24), 24627–24637 (2011).

#166974 - $15.00 USD Received 18 Apr 2012; revised 25 May 2012; accepted 26 May 2012; published 8 Jun 2012

13. W. Amaya, D. Pastor and J. Capmany,"Modeling of a time-spreading OCDMA system including non-perfect time gating, optical thresholding, and fully asynchronous signal/interference overlapping," J. Lightwave Technol. **26**, 768–776 (2008).

## 1. Introduction

Coherent Optical Code Division Multiple Access (C-OCDMA) systems have been demonstrated in different network contexts and applications like multiuser optical access networks or optical headers en/decoding in Photonic Label Switching (PLS) networks [1–4].C-OCDMA techniques can employ both the amplitude and/or the optical phase to construct the codified signal from the data pulses at the encoder. After transmission the decoder reconstructs the original data reversing the process. For the techniques based in Time Spreading (TS) concepts, also named Direct Sequence (DS), the original input signal is a short pulse which is encoded into a sequence of N sub-pulses (copies) named "chips" containing the code-word information into their optical phase. At the decoder end this sequence goes through a replica of the encoder with time axis rotated and with conjugated phases respect to the encoder to reconstruct the original pulse. This process requires intrinsically very short time optical pulses (i.e. broad band spectrums) to be codified and recovered with enough quality, and therefore this type of signals are strongly affected by the chromatic dispersion or GVD (Group Velocity Dispersion) present in the optical network even for short distances [5]. For example, TS encoded signals composed by Gaussian chips of 5 ps time width will suffer a broadening due to GVD up to 21.6 ps just only for10 km of standard fiber ($\beta_2 = -21 ps^2/km$). This time broadening leads to a strong degradation of the en/decoded signals due to the time overlapping between individual chips of the transmitted TS sequence.

In OCDMA literature this problem has been overcome generally employing Dispersion Compensation Fiber (DCF) coils or devices like Linearly Chirped Fiber Bragg Gratings (LCFBG) to turn the complete transmission network into a free of GVD case. These approaches imply additional devices on the system, higher optical losses and costs. One alternative approach to overcome the GVD impact based on decoders with twofold functionality, standard en/decoding and GVD compensation, was proposed theoretically and by simulation [6].Subsequently, we demonstrated experimentally the concept for Coherent DS-OCDMA encoders based on SSFBG (Super Structured Fiber Bragg Grating) of low reflectivity [7].

In this paper we present important improvements on these devices in two aspects. First, we demonstrate GVD dispersion compensation added to Coherent DS-OCDMA en/decoding in both extremes of the system sharing out the GVD compensation functionality between encoder and decoder devices. Shared GVD compensating devices require shorter SSFBG which are easier to fabricate and more stable with temperature [8].Moreover, shared GVD en/decoders are able to compensate different fiber lengths and they can be combined to demonstrate interoperation and increased network flexibility. The second important upgrade of the proposal introduces the High Reflectivity (HR) regime for the encoders and decoders.HR devices provide lower insertion losses but they suffer strong signal fading along the device and multiple reflections which cannot be neglected and must be compensated into the device design [9, 10].Here we present the results for the design of HR encoders with added GVD compensation capability employing DLP method [11] and their experimental verification achieving more than 9 dB of insertion loss reduction for each device.

In section 2 we discuss the en/decoder design procedures for low and high reflectivity devices with added GVD compensation features. Then in section 3 we present the spectral characterization of the SSFBG devices and the encoded optical sequences with and without the effect of GVD. In section 4 the complete set of designed and fabricated en/decoders are tested from a system point of view obtaining autocorrelation and cross-correlation signals for a complete range of fiber length to verify the GVD compensation principle.

#166974 - $15.00 USD Received 18 Apr 2012; revised 25 May 2012; accepted 26 May 2012; published 8 Jun 2012

## 2. Design and fabrication of GVD compensated SSFBG en/decoders

The en/decoding process in presence of GVD can be represented as a concatenated linear process employing the spectral description of the encoder/decoder pair and the equivalent transfer function of the fiber GVD

$$H_{tot}(\omega) = H_{encod}(\omega)H_f(\omega)H_{decod}(\omega) = H_{encod}(\omega)\cdot\exp\left[-j\beta_2 L(\omega-\omega_0)^2/2\right]\cdot H_{decod}(\omega) \qquad (1)$$

where $\omega_0$ is the central pulsation of the system and $\beta_2$ the first order dispersion of the link. Notice that second order dispersion $\beta_3$ have been neglected, but all the remaining considerations are valid for any type of dispersion. From the time response perspective the output signal can be described as the convolution of the three elements composing the system and the input pulse $s_{in}(t)$ as

$$s_{out}(t) = s_{in}(t)\otimes h_{encod}(t)\otimes h_f(t)\otimes h_{decod}(t) \qquad (2)$$

In order to compensate the link dispersion, a GVD compensation element $H_{GVD\_comp}(\omega) = H_f(\omega)^* = \exp\left[j\beta_2 L(\omega-\omega_0)^2/2\right]$ has to be inserted at any point in the chain because the system can be considered linear. In that way, we can insert the GVD compensating impulse response $h_{GVD_comp}(t)$into expression (2) and to group with encoder or decoder impulse response respectively. As mentioned, we presented a practical proof of concept including the compensating transfer function $H_{GVD\_comp}(\omega)$, in the encoder device to compensate around 11.19 km of standard fiber [6].Moreover this GVD compensation technique can be shared between both network extremes due to the linearity condition splitting the total GVD in a certain proportion, reducing the amount dispersion to be compensated at each device and therefore leading to shorter devices.

For the compensated en/decoders design we started assembling an ideal impulse response $h_{en/decod}(t)$ based on a 63 chips code word (code information into the bipolar phase) from the Gold Codes family. The chip time spacing was set to 5.8 ps and the chip shape was Gaussian with a time width slightly shorter than the chip time spacing to avoid interference between chips. The next step was the definition of the $h_{GVD_comp}(t)$function and the convolution of both signals to perform the desired impulse response $h_{En/Dec\_comp}(t)$. In that way the compensated en/decoders impulse response is composed by the broadened set of initial chips and their mutual interference. This apparently like-noise response contains all the code information and will be reconstructed after propagation through the proper amount of GVD.

As mentioned in the introduction, the majority of the proposed SSFBGs for CDS-OCDMA have been in low reflective regime (Born approximation) to avoid power depletion and multiple reflection effects. In this case, the desired impulse response can be translated directly to the Bragg perturbation complex coupling coefficient $q(z) = \kappa(z)\exp(j\phi(z))$(i.e $.\kappa(z) \propto |h_{GVD_comp}(t)|$and$\phi(z) = angle(h_{GVD_comp}(t))$, with $z = (t \times v_g)/2$), where $\kappa(z)$ is the coupling coefficient amplitude,$\phi(z)$contains the phase changes respect to the Bragg period and $v_g$ is the group velocity at the Bragg wavelength $\lambda_B$. Finally the general form of the refractive index along the device is$n(z) = n_0 + \Delta n_{DC}(z) + \Delta n_{AC}(z) \times \cos(2\pi/\Lambda_B + \phi(z))$where $n_0$ is the base refractive index of the fiber, $\Delta n_{DC}(z)$is the averaged refractive index increment (DC index), and $\Delta n_{AC}(z)$ is the amplitude of the Bragg perturbation related with $\kappa(z) = (\pi/\lambda_B)\cdot\Delta n_{AC}(z)$ [10].

Figure 1 shows the amplitude of complex coupling coefficient $|q(z)|$ of five designed devices and the phase changes of $q(z)$for the first compensating decoder. The case of whole GVD compensation ($\beta_2 L = -245.5$ ps$^2$) allocated in one extreme (encoder or decoder) is shown in Fig. 1(b) and 1(c). We selected the decoder for the demonstration without loss of generality. In this case the encoder is the standard one (as shown in Fig. 1(a) with label C1). As mentioned before for the compensated impulsive response the amplitude and phase changes of $q(z)$ contain the code information (originally being bipolar phase changes) affected

#166974 - $15.00 USD Received 18 Apr 2012; revised 25 May 2012; accepted 26 May 2012; published 8 Jun 2012

by the multiple interferences of the $h_{GVD\_comp}(t)$ function. We can observe this into the designed phase response of $q(z)$in Fig. 1(b).

The case of shared GVD between encoder and decoder with approximately half GVD amount ($\frac{1}{2}\beta_2 L$) is shown in Fig. 1(d) and 1(e). We show in this case the designed compensated encoders (labels C1 & C2 + GVD/2 in the figure), and the decoders present the same $|q(z)|$ behavior but rotated in z axis.

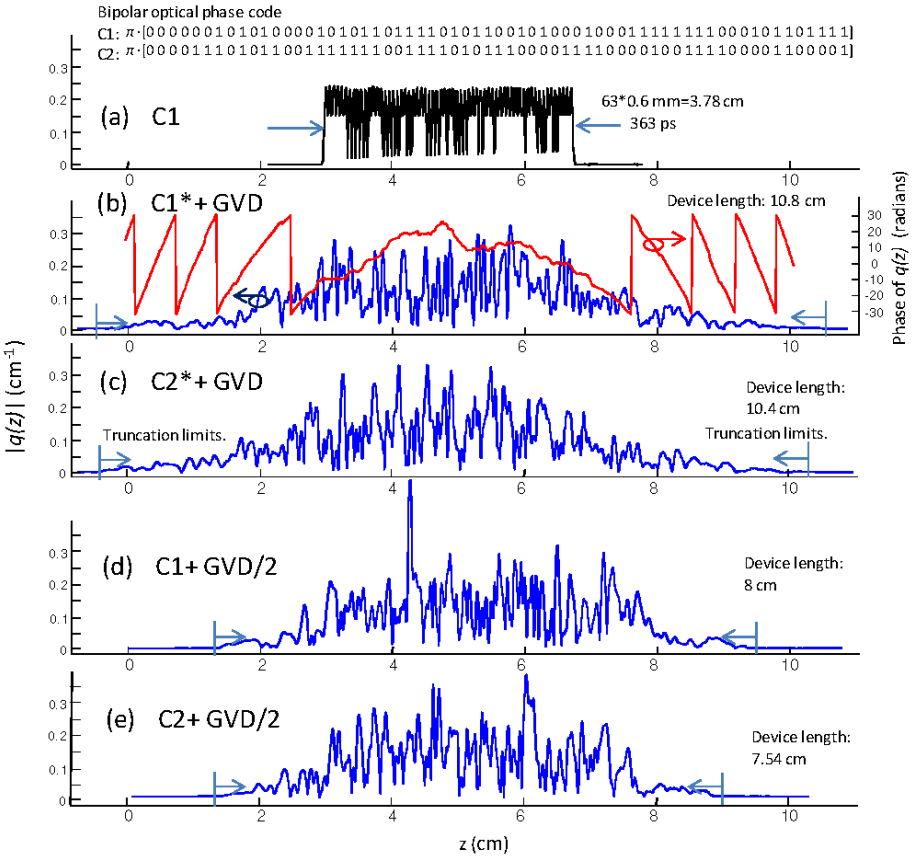


Fig. 1. Amplitude of complex coupling coefficient in the Low Reflectivity regime. (a) Standard non GVD compensated encoder C1, (b) Compensated decoder C1* + GVD (amplitude and phase),(c) Compensated decoder C2* + GVD, (d) Shared compensated encoder C1 + GVD/2,(e) Shared compensated encoder C2 + GVD/2.

Notice that as we use bipolar codes, standard encoder and decoder devices (like C1 in the figure) are exactly equal, it means that the encoder can be used as a decoder device by changing the input ports. However, in the case of GVD compensated devices, despite that code is bipolar, each encoder and decoder must be designed separately because the optical phase response containing the GVD compensation is port sensitive.

In the case of high reflectivity SSFBGs [9], a direct translation of the desired response $h_{En/Dec\_comp}(t)$ into $q(z)$results in a degradation of the effectively reflected response due to power depletion and multiple reflections. HRSSFBGs $q(z)$ values must be calculated by means of synthesis methods that start from the desired response $h_{En/Dec_comp}(t)$to obtain iteratively layer by layer the specific $q(z)$function that provides the desired impulse response [10].We employed Discrete Layer Peeling (DLP) method [11] that performs optimum results with low computing time requirements. The designs shown in Fig. 1 correspond with the low reflectivity devices where the maximum amplitude of the coupling coefficient $q(z)$ fluctuates

#166974 - $15.00 USD Received 18 Apr 2012; revised 25 May 2012; accepted 26 May 2012; published 8 Jun 2012

around ~0.25 $cm^{-1}$ . This coupling value was taken as the limit that ensures a power depletion lower than 2% in amplitude along the 63 chips in the impulse response of the device C1. In the case of HR devices we forced the synthesis method to find the solutions for *q(z)* starting from the same ideal impulse responses *h(t)* employed for the LR regime devices but multiplied by a factor of × 3. The obtained HR *q(z)* profiles where three times more intense on average (~0.75 $cm^{-1}$) but also included the required corrections to compensate the strong multiple reflections and power depletion. Standard non GVD compensated en/decoder and HR en/decoder devices have *q(z)* profiles extended up to twice the length of the equivalent LR device because the multiple reflections between chips falling out the chips region are corrected by the synthetized *q(z)* [10]. However, due to the already broadened impulse response of the compensated devices ($h_{En/Dec\_comp}(t)$),the HR and GVD compensated decoders presented just only ~1cmincrease in length respect to their LR counterpart (~10.8 cm in Fig. 1(b), and also slight modifications of the *q(z)*shape at the last ~2cmon the right edge that corrects the multiple reflections.

Finally, complex coupling coefficient *q(z)* must be fabricated into the photosensitive optical fiber core by Ultra Violet (UV) fringe pattern irradiation [12]. With this objective *q(z)* is discretized into a number of steps depending on the size of the UV spot and the device length. For example, the 10.8 cm long devices were discretized into720 steps spaced $\Delta z$ = 150μm. Discretized values of *q(z)*(modulus and phase)were imprinted by means a focused UV beam and a phase mask with fixed period ($\Lambda_M$ = 1070.4 nm) which moves jointly respect to a static photosensitive fiber. An optical shutter controls the UV illumination time and it turns off the beam during the movement step by step along the fiber. Amplitude values of *q(z)* are adjusted by diphase of the Bragg period ($\Lambda_B = \Lambda_M /2$) between the two expositions that is controlled by the proper displacement between them. Relative phase change between two discrete values *q(z)*and $q(z + \Delta z)$is achieved also by the proper displacement of the fringe pattern between the two expositions for *q(z)* and the second couple for $q(z + \Delta z)$. UV beam power and exposition time was constant to ~50 mW and ~200 ms along the whole device to ensure a constant profile of the averaged refractive index (DC index)to avoid deleterious Bragg phase distortions into the fabricated devices. UV mirrors, lenses and finally the phase mask are assembled over a translation stage that provides ± 5 nm of accuracy in the exposition displacement that ensures Bragg phase errors lower than $\pi/50$. Optimized tracking of the UV beam over the photosensitive fiber is also important in such as long devices. We achieved this by measuring the fiber fluorescence to the UV exposures and a closed loop actuation over the last mirror that is mounted on a piezoelectric transducer.

## 3. Spectral and temporal characterization of the GVD compensator en/decoders

Prior to the presentation of the system measurements, where we will show the whole en/decoding process, we present in this section the characteristics of the en/decoders in both the temporal and the frequency domain. We fabricated 10 different en/decoder devices, 6 for code 1 and 4 for code 2 divided as it is shown in Table 1.

**Table 1. List and Description of En/Decoder Devices Fabricated**

| Label | Code | Reflectivity | GVD compensation of SSMF length (km) |
|---|---|---|---|
| C1 *(Fig. 1(a))* | 1 | Low | 0 |
| C1DA *(Fig. 1(d))* | 1 | Low | 5.4 |
| C1DA* | 1 | Low | 5.4 |
| C1DB* *(Fig. 1(b))* | 1 | Low | 11.4 |
| C1H | 1 | High | 0 |
| C1DH* | 1 | High | 11.4 |
| C2 | 2 | Low | 0 |
| C2DA *(Fig. 1(e))* | 2 | Low | 5.4 |
| C2DA* | 2 | Low | 5.4 |
| C2DB* *(Fig. 1(c))* | 2 | Low | 11.4 |

#166974 - $15.00 USD Received 18 Apr 2012; revised 25 May 2012; accepted 26 May 2012; published 8 Jun 2012

Table 1 shows the device identification (label), the assigned code-word inside the 63 chip Gold set, the reflectivity regime (Low or High), and the amount of compensated dispersion expressed in terms of SSMF length (11.4 km → $\beta_2 L = -245.5$ ps$^2$). With these devices we can test,as it will be detailed in next section, the simultaneous GVD compensation and en/decoding process for different link length combinations from 5.4 km up to 16.8 km in addition to the non GVD compensated case.

As said in the previous section, the GVD compensated en/decoder frequency response was obtained by the product of the compensation transfer function $H_{GVD_comp}(\omega)$and the encoder $H_{encod}(\omega)$(or decoder) function. Therefore, the GVD compensated en/decoder spectral phase response corresponds to the summation of the phase responses, i.e. $\phi_{En/Dec\_comp}(\omega) = \phi_{En/Dec}(\omega) + \phi_{GVD\_comp}(\omega)$. In the same way, the group delay response of the GVD compensated en/decoder is just the sum of the group delay of its individual constituents. On the other hand the amplitude response should remain unaltered because of the all-pass characteristic of $H_{GVD\_comp}(\omega)$.

In Fig. 2 we can see the experimentally obtained responses for a standard decoder and the corresponding compensated decoder for $\beta_2 L = -245.5$ ps$^2$(or DL = 192.5 ps/nm) in the high reflectivity domain implementing code 1 (C1H and C1DH*). We observe that the amplitude response has a similar behavior for both devices (Fig. 2(a) and 2(b)), obtaining similar reflectivity values. With regard to the group delay measurements, Fig. 2(c) and 2(d) shows respectively the results for the fabricated standard encoder and the GVD compensated decoder. The standard encoder group delay presents the typical strong fluctuations around its mean value (in this case it was normalized to zero after measurement). The compensated device, as expected, presents the added responses of the standard en/decoder and the linear group delay variation corresponding to the design parameter DL.

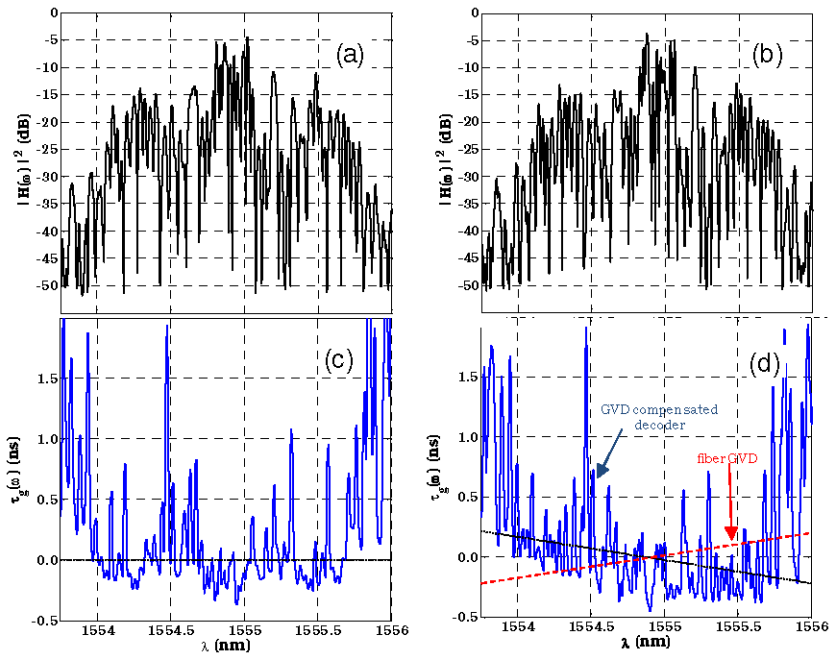


Fig. 2. (a) Spectral amplitude of high reflectivity encoder, (b) Spectral amplitude of high reflectivity compensated decoder, (c) Group delay of the standard decoder, (d) Group delay of the high reflectivity compensated decoder.

In the temporal domain, we can see that the impulse responses for the encoder in the low (Fig. 3(a)) and the high reflectivity regime (Fig. 3(b)) have the same shape with 363ps

#166974 - $15.00 USD Received 18 Apr 2012; revised 25 May 2012; accepted 26 May 2012; published 8 Jun 2012

duration, and that the insertion loss (IL) is 11dB greater for the low reflectivity device. On the other hand, the compensated decoder impulse response (Fig. 3(c) and 3(d)) presents a dispersed-like shape with a total duration of 580ps, which is caused by the dispersive phase inscribed in the device. Nevertheless, the shape of the amplitude impulse response of the ensemble formed by the fiber link and the compensated decoder (Fig. 3(e) and 3(f)) corresponds perfectly with the time axis rotated shape of the encoder. Hence, the compensated encoder will provide a perfectly matched signal for the design link dispersion (in this case $-245.5$ ps$^2$).Again, the shapes of the high and low reflectivity devices are the same, but with a difference of 9.8 dB in IL.

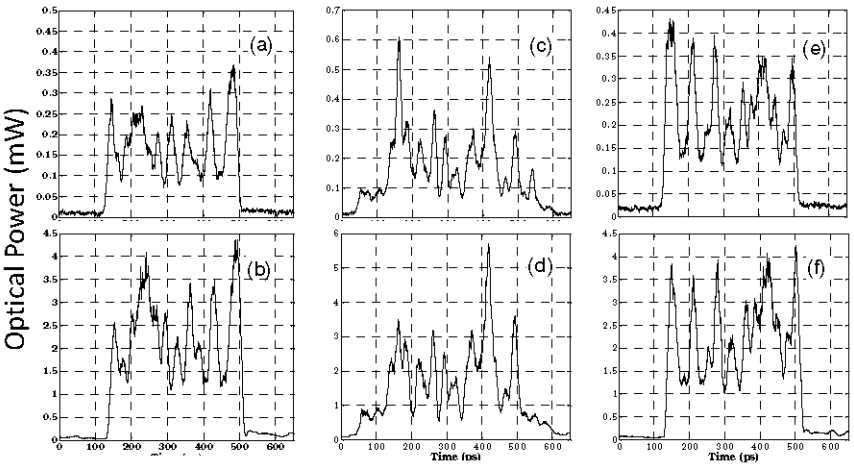


Fig. 3. Squared Amplitude temporal responses: (a) Encoder low reflectivity (C1) and (b) high reflectivity encoder (C1H). (c) Compensated decoder low reflectivity (C1DB*) and (d) high reflectivity compensated decoder (C1DH*). (e) Optical fiber link (11.4 km) + compensated decoder for low reflectivity (C1DB*) and (f) and optical fiber link (11.4 km) + high reflectivity decoder (C1DH*).

For the previous example, the encoder should provide an amplitude temporal impulse response formed by 63 pulses separated 5.8 ps. The figures experimentally obtained present strong amplitude variations which should not be present in bipolar phase encoding. This effect is due to the interference between adjacent chips with 0 to $\pi$ phase change (or vice versa) and is caused by the higher pulse width than chip time of the available optical sources for the experiment. Please note that the figure resolution is limited by the sampling oscilloscope electrical bandwidth (80 GHz).

## 4. En/decoding system measurements

The performance experimental demonstration of the dispersion compensation devices was done employing the setup showed in Fig. 4. The optical source was a Mode Locked Laser (MLL) switched at 10 GHz and then decimated by a modulator and a pulse pattern generator up to obtain a bit rate of 1.25 GHz with a pulse width of 8 ps. This signal is amplified, applied to the encoder by a circulator and amplified again. The two first amplifiers were fixed gain (20 dB) EDFAs. Then, the encoded signal is applied to a set of variable length optical fiber coils (SSMF) and amplified by means of variable gain EDFA to compensate the insertion losses. Finally, the signal is applied to the decoder through the last circulator and detected employing a sampling oscilloscope with 80 GHz of electrical bandwidth. Each encoder and decoder was inserted in a controlled temperature box, for tuning the mismatch in wavelength produced in the fabrication process and to keep the stability of the system during the measurements.

#166974 - $15.00 USD Received 18 Apr 2012; revised 25 May 2012; accepted 26 May 2012; published 8 Jun 2012

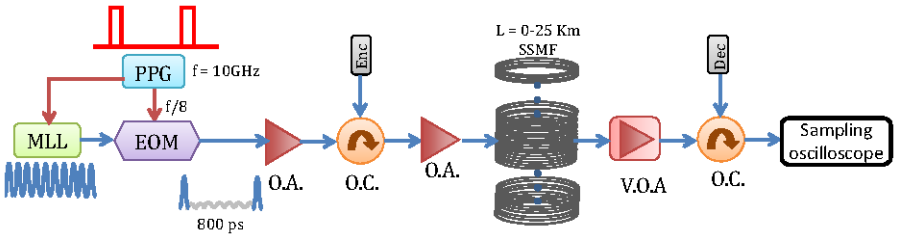


Fig. 4. Experimental system setup. Mode locked laser (MLL), Electro-Optical modulator (EOM), Pulse pattern generator (PPG), Optical amplifier (O.A.), Optical circulator (O.C.), Variable optical amplifier (V.O.A.), Standard single mode fiber (SSMF).

Figure 5 shows the obtained results with a representative combination of encoders C1 and C2 and the decoder C1DB*. In this case the labels indicate that the encoders are standard devices without GVD compensation implementing code-word 1 and 2 and with low reflectivity. On the other hand the decoder is designed with code-word 1 (conjugated as it corresponds with a decoder), with dispersion compensation of 11.4 km ('DB' case) and also low reflectivity. We can see that the maximum auto correlation peak (C1 & C1DB*) is obtained just for the designed distance, 11.4 km, and as distance increases or decreases the power peak decreases up to almost disappear due to the non compensated amount of GVD (Fig. 5(a)). The ACP peak power reduction is strong even for low fiber length discrepancies from the optimum compensation length reducing up to 50% just for ± 3 km. Nevertheless, the cross correlation signal XC (C2 & C1DB*) keeps the same mean power value for all distances. It is important to note that, as we can see in Fig. 5(b), the XC results for the optimum compensating length remain unaltered and bounded to the expected values for the standard devices (with no GVD compensation) which proves the feasibility of the compensating techniques also from the point of view of code orthogonality.

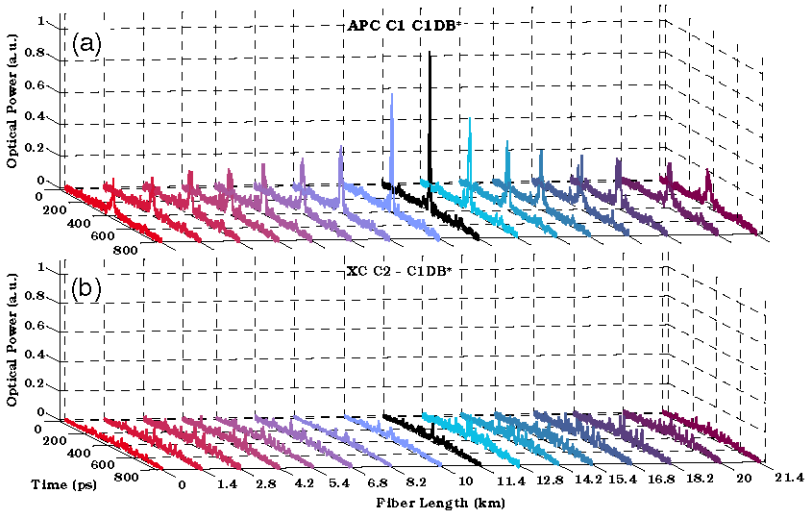


Fig. 5. Experimental results for the combinations: (a) encoder C1 with decoder C1DB* (ACP), (b) C2 with C1DB* (XC).

Additionally to the shown configuration we carried out different combinations with the 10 en/decoder devices to prove the technique feasibility and to demonstrate the shared GVD compensation and the GVD compensation in high reflectivity regime. The multiple measured configurations are summarized in a double input table Encoder/Decoder (Table 2).The up-left corner section groups the ACP signals of encoders and decoders designed for the

#166974 - $15.00 USD Received 18 Apr 2012; revised 25 May 2012; accepted 26 May 2012; published 8 Jun 2012

implementation of code 1with different GVD compensations and the down-left section the XC signals resulting from encoders with code 2 and decoders with code 1 (same GVD cases also). The equivalent structure is followed for ACPs of code 2 (up-right) and XC signals (down-right). In the center of the table is depicted the high reflectivity case also measured.

**Table 2. Encoder and decoder combinations characterized. Colors indicate the correspondence with traces in following figures.**

| En\Dec | C1* | C1DA* | C1DB* | C1DH* | C2* | C2DA* | C2DB* |
|---|---|---|---|---|---|---|---|
| C1 | ACP C1 0 km | ACP C1 5.4 km | ACP C1 11.4 km | | XC C1C2 | XC C1C2 | XC C1C2 |
| C1DA | | ACP C1 10.8 km | ACP C1 16.8 km | | | XC C1C2 | XC C1C2 |
| C1H | | | | ACP C1 11.4 km | | | |
| C2 | XC C2C1 | XC C2C1 | XC C2C1 | XC C2C1 | ACP C2 0 km | ACP C2 5.4 km | ACP C2 11.4 km |
| C2DA | | XC C2C1 | XC C2C1 | | | ACP C2 10.8 km | ACP C2 16.8 km |

For all the described combinations we carried out en/decoding measurements similarly to the ones shown in Fig. 5 and from them we process the traces to extract the two main system performance parameters for each value of fiber length inserted into the link: 1) The ACP power just only taking the peak value and 2) the averaged value of the XC power measured along the 800 ps time axis. We take averaged XC values attending to general assumption that the XC signals of different interfering users (located randomly) will impact over the ACP signal uniformly distributed in time along the whole XC range [13].

Figure 6(a) shows the ACP values ($P_{ACP}$) and the averaged XC values ($P_{XC}$) described for each case of the code 1 with low and high reflectivity (rows 1, 2 and 3 in Table 2). In the same way Fig. 6(b) shows the results for code 2 with low reflectivity (rows 4 and 5 in Table 2). In all the measurements the incoming averaged optical power to the decoder was adjusted to a fixed value in order to compensate the different insertion losses of the fiber coils and the feasible slight differences between encoders due fabrication tolerances. Also the en/decoding process was carried out in a symmetrical way (i.e. both ACPs for C1 and C2 were performed and also the corresponding crossed signals XC C2C1 and XC C1C2), to ensure that the interference relations were that correspondent to a completely functional situation. Finally, the results are shown normalized respect to the maximum value of $P_{ACP}$ for each case.

#166974 - $15.00 USD Received 18 Apr 2012; revised 25 May 2012; accepted 26 May 2012; published 8 Jun 2012

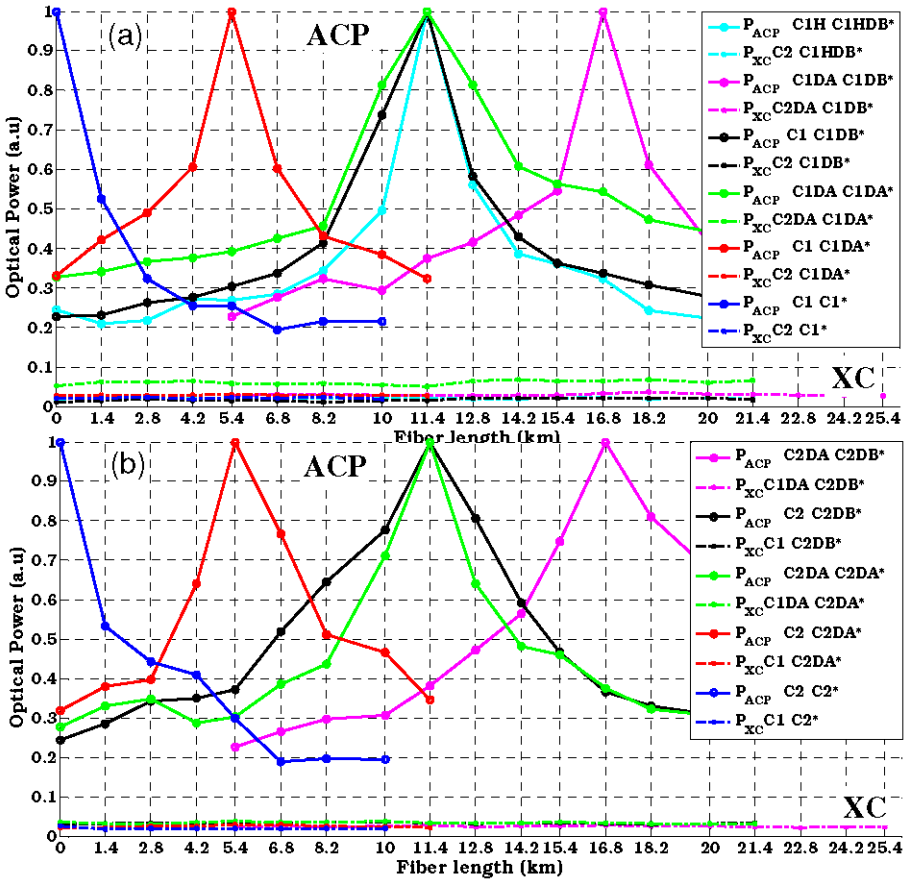


Fig. 6. Experimental results for the configurations of encoder and decoder devices with code 1 (a) and with code 2 (b).

From the final results shown in Fig. 6we can extract some conclusions. First, the non compensated case (C1 C1* and C2 C1*) shows the expected strong degradation of the ACP peak due GVD even for short fiber lengths (blue traces). The ACP peak power reduces to half for 1.4 km and up to 20% for 6.8 km. The XC signals maintain their original levels (GVD does not reduce the XC averaged power just only reorder the energy inside the XC signal time region). The same results are obtained for code 2(C2 C2* and C1 C2*).The consequence of that is a strong quality reduction due to the increase of the crosstalk ratio $\xi = \langle P_i \rangle / P_d$ expected ideally for a given code family, where $P_d$is the "data" decoded and $\langle P_i \rangle$ is the average interfering power [13].In our experimental verification the crosstalk ratio can be associated to the modified ratio $\xi' = P_{XC} / P_{ACP}$ where the limit due to the electrical bandwidth of the sampling oscilloscope is enclosed. We can see that the achieved $\xi'$ for the non compensated devices (blue traces) for 0 km is around ~30 and it can be taken as reference for the other components.

Secondly, the compensated device combinations that employ a standard encoder C1 o C2 and a GVD compensated decoder (CxDA* red trace and CxDB* black trace) provide almost perfect recovery of the ACP peak for the design lengths 5.4 km and 11.4 km respectively. Notice that the XC signals for these two compensated cases do not increase respect to the standard cases. Similar results are obtained for C2 where we can only observe a slight difference in the decaying slope around the optimum peaks. This behavior was investigated

#166974 - $15.00 USD Received 18 Apr 2012; revised 25 May 2012; accepted 26 May 2012; published 8 Jun 2012

by simulation and it was found that the decaying slope around the peaks can vary slightly depending on the specific code-word employed.

The third conclusion comes from the cases where we employ a GVD compensated device in both encoder and decoder ends (i.e. CxDA- CxDA* green trace and CxDA - CxDB* magenta trace). We can see how the shared GVD compensation provides the optimum ACP at the summation of the compensating objectives of each device, ~10.8 km and 16.8 km respectively. The maximum ACP for the 5.4 km + 5.4 km compensation case was measured for 11.4 km due to the limited fiber coil combinations available. Finally we show in Fig. 6(a) the results obtained for the high reflectivity encoder with GVD compensating features. It presets perfect recovery of the ACP for the objective length of 11.4 km and the XC averaged signal maintains at the same levels than the ones obtained for low reflective devices. This fact proves the feasibility of that type of GVD compensated devices which moreover reduce drastically the insertion losses as detailed in the previous section.

We have demonstrated GVD compensated en/decoders up to fiber lengths of 11.4 km for a single device or 16.8 km for a combination of encoder and decoder. This fiber ranges are compatible with LAN environments based on passive star coupler or with metropolitan access networks where the Central Office (CO) is connected through a the feeder fiber section with a passive Remote Node (RN) and the users or Optical Network Terminals (ONT) are connected to RN through the distribution fiber section. For this application en/decoders placed at CO compensate the GVD amount of feeder section and en/decoders at ONUs compensate the distribution section. OCDMA en/decoding have been proposed also for OCDMA/WDM path networks [2] or applied to header recognition in Photonic Label Switching (PLS) networks [3]. In this case the GVD amount from the fiber span between two cross-connects can be shared between en/decoders at two nodes. Fiber span in PLS or path networks paradigm increase up to 50-80 km [3] and therefore shared GVD devices may be designed for 25-40 km each leading to longer SSFBGs. Nevertheless, notice that demonstrated devices compensate up to ~284 ps/nm (16.8 km employing SSMF) therefore the compensated fiber range increases up to 57-70 km in the case of using Non-Zero Dispersion Shifted Fibers (4-5ps/nm km).

## 5. Conclusion

We have proposed, fabricated and demonstrated experimentally a set of Coherent DS-OCDMA en/decoders based on SSFBGs which are able to compensate the fiber chromatic dispersion at the same time that they perform the en/decoding task. The simultaneous en/decoding and dispersion compensation ability have been demonstrated concentrated into one device or shared between encoder and decoder in both extremes of the system. Shared GVD devices require shorter SSFBG which are easier to fabricate and more stable with temperature. Also en/decoders designed to compensate different fiber lengths have been combined to demonstrate interoperation and increased network flexibility. Moreover, we have designed this type of devices into the High Reflectivity regimen by means of FBG synthesis algorithms providing lower insertion losses. We verified experimentally excellent results for this HR and GVD compensated devices achieving more than 9 dB reduction of insertion loss for each device.

## Acknowledgments

This work was supported by the Spanish Government project TEC 2009-12169, and the Valencian Government under the projects ACOMP/2012/023and FPA/2012/009.

#166974 - $15.00 USD Received 18 Apr 2012; revised 25 May 2012; accepted 26 May 2012; published 8 Jun 2012